ACS OMEGA

http://pubs.acs.org/journal/acsodf

Article

Influence of Hydrotropes on the Solubilities and Diffusivities of Redox-Active Organic Compounds for Aqueous Flow Batteries

Yingchi Cheng, Derek M. Hall, Jonathan Boualavong, Robert J. Hickey, Serguei N. Lvov, and Christopher A. Gorski*

Cite This: *ACS Omega* 2021, 6, 30800−30810

Read Online

ACCESS | Metrics & More | Article Recommendations | Supporting Information

ABSTRACT: In this study, we explored the extent to which hydrotropes can be used to increase the aqueous solubilities of redox-active compounds previously used in flow batteries. We measured how five hydrotropes influenced the solubilities of five redox-active compounds already soluble in aqueous electrolytes (≥0.5 M). The solubilities of the compounds varied as a function of hydrotrope type and concentration, with larger solubility changes observed at higher hydrotrope concentrations. 4-OH-TEMPO underwent the largest solubility increase (1.18 ± 0.04 to 1.99 ± 0.12 M) in 20 weight percent sodium xylene sulfonate. The presence of a hydrotrope in solution decreased the diffusion coefficients of 4-OH-TEMPO and 4,5-dihydroxy-1,3-benzenedisulfonate, which was likely due to the increased solution viscosity as opposed to a specific hydrotrope−solute interaction because the hydrotropes did not alter their molecules' hydraulic radii. The standard rate constants and formal potentials of both 4-OH-TEMPO and 4,5-dihydroxy-1,3-benzenedisulfonate remained largely unchanged in the presence of a hydrotrope. The results suggest that using hydrotropes may be a feasible strategy for increasing the solubilities of redox-active compounds in aqueous flow batteries without substantially altering their electrochemical properties.

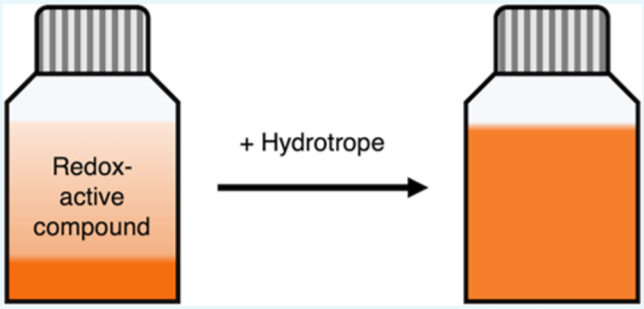

INTRODUCTION

Redox flow batteries are a promising approach for balancing temporal differences between electrical supplies and demands created by electricity production from intermittent renewable resources (e.g., solar and wind).[1−4] Redox flow batteries store and produce energy using electrolytes containing soluble redox-active compounds that are reversibly oxidized and reduced at electrode surfaces.[5,6] The main goal in developing redox flow batteries is minimizing their costs, with the U.S. Department of Energy having set a capital cost target of USD $150 per kWh by 2023.[7] First-generation redox flow batteries used vanadium redox couples, which provided sufficiently high aqueous solubilities and cell voltages but were expensive due to the high price of vanadium.[8] To decrease costs, researchers began using organic redox-active compounds as opposed to metal-based compounds.[9−12] However, the energy densities of organic-based aqueous redox flow batteries have been limited by low solubilities of organic compounds in aqueous electrolytes.[1,12−14]

To date, the main approach to increase the energy densities of organic-based aqueous redox flow batteries has been to alter the functional groups on organic compounds to tune their solubilities, reduction potentials, and/or the number of electrons transferred.[14−18] For example, substituting and repositioning the functional groups on quinone compound shifted its reduction potentials by up to 1.17 V[19] and increased its solubility by over an order of magnitude.[6,14,20] Similarly, replacing methyl groups on methyl viologen with more hydrophilic ammonium functional groups increased the number of usable electron-transfer steps from 1 to 2.[18,21] Although such molecular engineering techniques show promising energy density improvements, they require organic syntheses with multiple steps, which can be time consuming and difficult to scale up.

An alternative, less studied approach to increase redox flow battery energy densities is to amend the aqueous electrolyte with a hydrotrope.[15,16] Hydrotropes are amphiphilic organic compounds most commonly used to increase the solubilities of sparingly soluble organic molecules.[22−28] Hydrotropes differ from surfactants in that they do not form micelles,[22,26] but the mechanisms by which they promote solubilization remain a topic of debate in literature.[24,26,27] Two recent flow battery studies used high concentrations of hydrotropes to successfully

Received: September 15, 2021
Accepted: October 19, 2021
Published: November 1, 2021

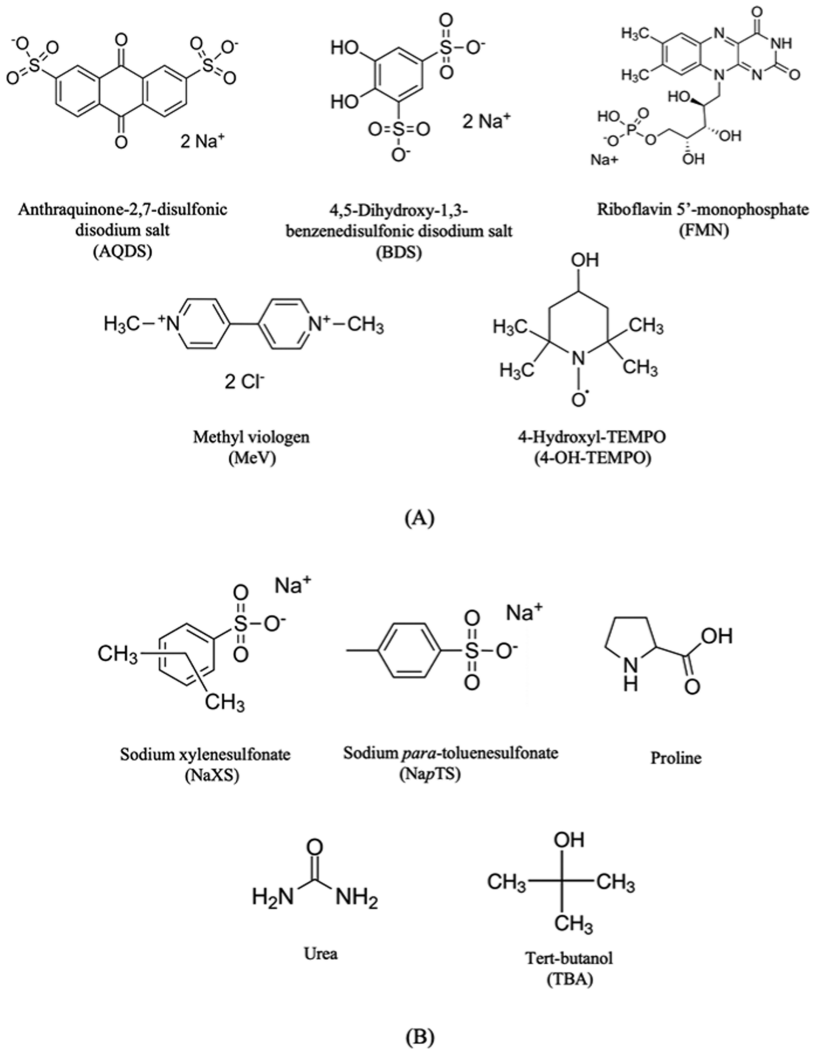

Figure 1. (A) Five redox-active organic compounds and (B) five hydrotropes used in this study.

increase the aqueous solubilities of organic redox-active compounds. The addition of 3.0 M hydrotrope nicotinamide (vitamin B3) increased the aqueous solubility of flavin mononucleotide from 0.1 to 1.5 M in 1.0 M KOH.[16] In another study, the addition of 4.0 M hydrotrope urea increased the solubility of hydroquinone (benzene-1,4-diol) from 0.5 to 1.5 M in deionized water.[15] In these studies, hydrotropes did not change the formal reduction potential values of the compounds. In the case of hydroquinone, urea did not significantly alter its diffusion coefficient, and it slightly decreased its standard rate constant.[15] These results indicate that hydrotropes may be an effective way to increase the solubilities of organic redox-active compounds in aqueous electrolytes when their initial solubilities are relatively low (≤0.5 M). What remains unclear is whether hydrotropes can also increase the solubilities of highly soluble redox-active compounds (>0.5 M) and, if so, how hydrotropes alter the electrochemical properties of the compounds.

The goal of this study was to identify promising combinations of hydrotropes and redox-active organic compounds that would increase the compounds' solubilities and to determine if their electrochemical properties would change. We surveyed five redox-active organic compounds previously used in aqueous redox flow battery studies: methyl viologen (MeV),[11] 4-OH-TEMPO,[11] anthraquinone-2,7-disulfonate (AQDS),[13,29,30] 4,5-dihydroxy-1,3-benzenedisulfonate (BDS),[29,30] and riboflavin-5′-monophosphate (FMN)[16] (Figure 1A) in the presence of five different hydrotropes: sodium xylenesulfonate (NaXS),[22] sodium *para*-toluenesulfonate (Nap TS),[22] proline,[22] urea,[15,28] and *tert*-butanol (TBA)[31] (Figure 1B). We selected the five organic compounds because they have shown promising electrochemical performance in the past flow battery study when used with different electrolyte conditions.[11,13,16,29,30] We chose the five hydrotropes because they were structurally diverse, they did not contain redox-active functional groups, and they were previously shown to increase the solubilities of hydrophobic organic compounds in past studies.[15,22,28,31]

We examined that the organic molecules' solubility changes in the presence of different concentrations of hydrotropes, ranging from 0 to 20 weight percent (wt %). Note that hydrotrope concentrations are conventionally expressed in units of weight percent in the literature.[22] For the hydrotrope−compound combinations that yielded the highest solubility increases, we used experimental electrochemical tests to determine how hydrotropes influenced the compounds' formal reduction potential ($E^{0'}$), diffusivity of the electrochemically active species (D), and the standard rate constant (k^0). We

https://doi.org/10.1021/acsomega.1c05133
ACS Omega 2021, 6, 30800−30810

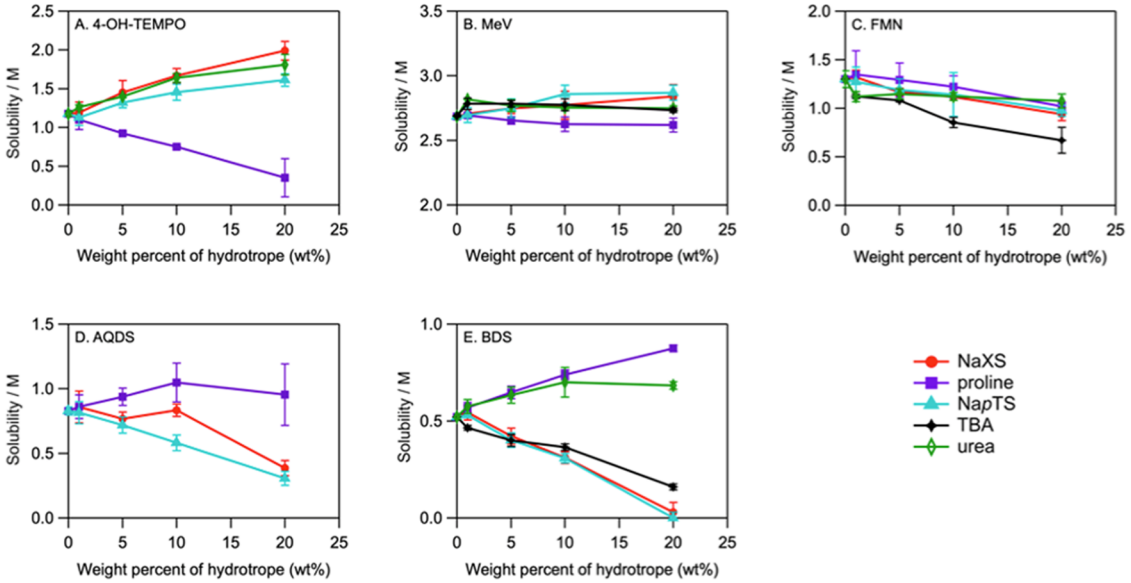

Figure 2. Aqueous solubilities of redox-active compounds as a function of hydrotrope concentration and type. The following acronyms are used in the figure; MeV: methyl viologen, FMN: riboflavin-5′-monophosphate, AQDS: anthraquinone-2,7-disulfonate, BDS: 4,5-dihydroxy-1,3-benzenedisulfonate, NaXS: sodium xylenesulfonate, Na*p*TS: sodium *para*-toluenesulfonate, and TBA: *tert*-butanol. Error bars represent the standard deviation for measurements made from triplicate reactors. Supporting electrolyte compositions: 1 M KCl (4-OH-TEMPO and MeV), 1 M KOH (FMN), and 1 M H_2SO_4 (AQDS and BDS).

used a cyclic voltammetry fitting algorithm to model our experimental data and determined values for $E^{0'}$, D, k^0, and the transfer coefficient (α). We also conducted the linear sweep voltammetry and electrochemical impedance spectroscopy using a rotational disk electrode setup to experimentally confirm the diffusion coefficient and standard rate constant values determined from cyclic voltammetry fitting algorithm.

RESULTS AND DISCUSSION

Influence of Hydrotropes on Aqueous Solubilities. The aqueous solubilities of the five redox-active compounds varied as a function of hydrotrope type and concentration, with larger solubility changes observed at higher hydrotrope concentrations (Figure 2). The aqueous solubilities of the redox-active compounds in the absence of a hydrotrope were similar to previously measured values, except for FMN, which was substantially more soluble in our study (1.3 M) than was previously reported (0.1 M) (Table S1).[11,16,29,32] Note the background electrolytes used in our experiments differed depending on the redox-active compound, as published redox flow battery studies employing the compounds were operated at different pH values (4-OH-TEMPO and MeV: 1 M KCl, pH ≈ 7; AQDS and BDS: 1 M H_2SO_4, pH ≈ 0; FMN: 1 M KOH, pH ≈ 14).[11,14,16,29] The solubility changes induced by a hydrotrope differed for each redox-active compound. For example, sodium xylenesulfonate (NaXS) significantly increased the solubility of 4-OH-TEMPO from 1.18 ± 0.04 M (0 wt %) to 1.99 ± 0.12 M (20 wt %), but NaXS significantly lowered the solubilities of AQDS from 0.83 ± 0.03 M (0 wt %) to 0.39 ± 0.06 M (20 wt %) and BDS from 0.52 ± 0.01 M (0 wt %) to 0.03 ± 0.05 M (20 wt %). In contrast, proline, another hydrotrope, exhibited the opposite trend; it increased the solubilities of BDS from 0.52 ± 0.01 M (0 wt %) to 0.88 ± 0.02 M (20 wt %) and of AQDS from 0.83 ± 0.03 M (0 wt %) to 1.05 ± 0.23 M (15 wt %), and it decreased the solubility of 4-OH-TEMPO (Figure 2A,D,E). Unlike the other redox-active compounds, MeV did not undergo substantial solubility changes in the presence of the hydrotropes (Figure 2B), which may be due to it having a higher aqueous solubility (2.69 ± 0.01 M) than the other compounds. Note we express the concentration of the hydrotrope using wt % due to the use of this convention in the hydrotrope literature.[22] A figure containing hydrotrope concentrations expressed in terms of molarity is in the SI (Figure S1).

The magnitude and direction of hydrotrope-induced solubility changes varied as a function of both the redox-active compound and the hydrotrope, which is consistent with observations made for sparingly soluble organic compounds solubilized by hydrotropes.[27,33−37] The lack of a universal trend is likely a consequence of multiple factors. First, hydrotropes are known to interact with and solubilize organic compounds via specific molecular interactions, such as $\pi-\pi$ interactions, with the strength of the specific attractive (or repulsive) forces depending on the chemical structures of the hydrotrope and compound.[24,33] Second, the electrolyte composition and solution pH values likely influenced hydrotrope−compound interactions. We used different pH values for different redox-active compounds, which could affect the hydrogen bonding and alter the structures of hydrotropes that undergo acid−base reactions [NaXS pK_A (for 3,4-dimethylbenzenesulfonate): 10.36;[38] proline $pK_{A,1}$: 2.0, $pK_{A,2}$: 10.6;[39]]. Third, the solubilities of AQDS and BDS may have been decreased in the presence of NaXS or Na*p*TS because both of these organic compounds are known to precipitate as sodium salts at low pH values.[29]

We observed that the largest solubility increases for (*a*) 4-OH-TEMPO in the presence of the hydrotropes NaXS, Na*p*TS, and urea and (*b*) BDS in the presence of the hydrotrope proline (Figure 2). Consequently, we focused on these compound−hydrotrope combinations in our subsequent experiments to understand how hydrotropes that increase the solubilities of redox-active organic compounds influence the

https://doi.org/10.1021/acsomega.1c05133
ACS Omega 2021, 6, 30800−30810

compounds' formal reduction potential values, diffusion coefficients, and interfacial electron-transfer kinetics.

Influence of Hydrotropes on 4-OH-TEMPO Electrochemical Parameters. We used cyclic voltammetry to examine how the presence of NaXS, Nap*T*S, and urea influenced $E^{0'}$, D, and k^0 of 4-OH-TEMPO (Figure 3A),

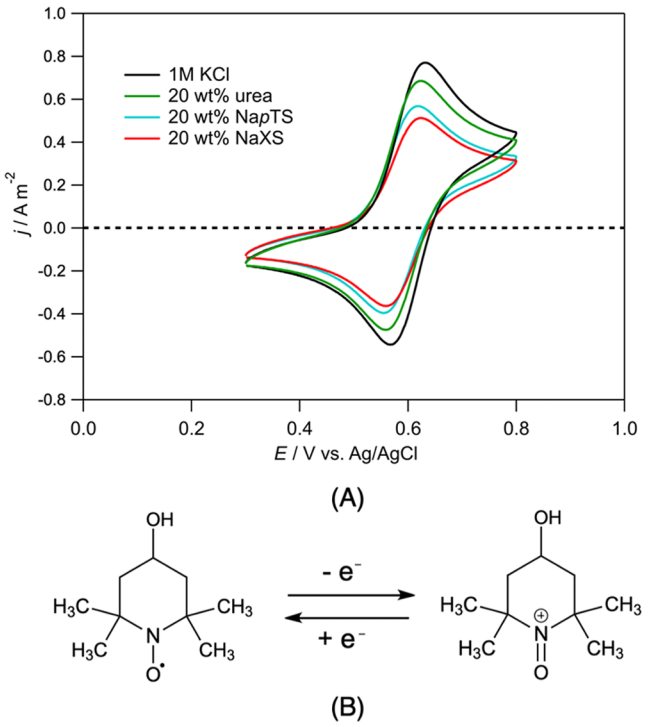

Figure 3. (A) Cyclic voltammograms of 1 mM 4-OH-TEMPO in 1 M KCl, 20 wt % urea, 20 wt % Nap*T*S, and 20 wt % NaXS at ν = 10 mV/s. The aqueous portions of hydrotrope solutions contained 1 M KCl. (B) Half-reaction of 4-OH-TEMPO.

which undergoes a single reversible electron-transfer reaction at circumneutral pH values to form an oxidized radical species ($E^{0'}$ = 0.59 V vs Ag/AgCl,[11] Figure 3B). The presence of the hydrotrope did not influence $E^{0'}$ values (no hydrotrope: 0.59 ± 0.00 V vs Ag/AgCl, 20 wt % NaXS: 0.59 ± 0.01 V, 20 wt % NapTS: 0.59 ± 0.00 V, 20 wt % urea: 0.59 ± 0.00 V), indicating that hydrotropes did not preferentially alter solvation energies (ΔG^0_{solv}) of the reduced or oxidized forms of 4-OH-TEMPO.[40] In control experiments lacking 4-OH-TEMPO, we confirmed that hydrotropes did not undergo any electron-transfer reactions over the same potential window (Figure S2). All four CVs were reversible at a scan rate of 10 mV/s. We calculated peak separation values, and they were close to the theoretical value for a reversible one-electron redox reaction at neutral pH (*peak separation*: no hydrotrope: 60 mV, 20 wt % NaXS: 62 mV, 20 wt % Nap*T*S: 61 mV, 20 wt % urea: 63 mV), indicating that the standard reaction rate constant (k^0) was sufficiently large relative to the diffusivities of both reduced and oxidized form of 4-OH-TEMPO (D_{red} and D_{ox}) to achieve reversible electron-transfer kinetics in the presence and absence of hydrotropes.[41] We found that peak currents were lower in the presence of a hydrotrope relative to the control condition lacking a hydrotrope (Figure 3A), which indicated that hydrotropes decreased the diffusivity of both 4-OH-TEMPO and the oxidized 4-OH-TEMPO species.

We collected CVs for each solution at several scan rates (0.001, 0.01, 0.05, 0.1, 0.5, and 1 V/s) to quantify the D and k^0 values of 4-OH-TEMPO in the presence and absence of a hydrotrope. We background subtracted the capacitive current from voltammograms using data collected for otherwise identical solutions lacking the redox-active compound and fitted the CVs of all scan rates simultaneously to a finite-element model described in the experimental section (Figure 4). We confirmed the accuracies of the values determined from the CVs for a subset of the conditions by performing linear sweep voltammetry measurements (LSV) using a rotating disk electrode cell and electrochemical impedance spectroscopy (EIS). The main advantage of performing cyclic voltammetry

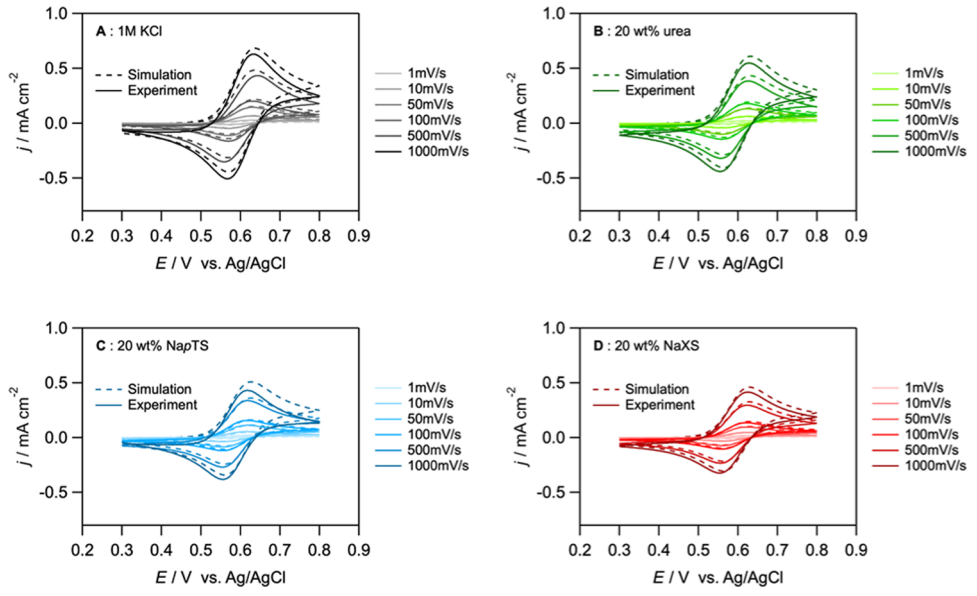

Figure 4. CV experimental results (solid lines) and simulation fits (dashed lines) for 1 mM 4-OH-TEMPO in (A) 1 M KCl, (B) 20 wt % urea in 1 M KCl, (C) 20 wt % Nap*T*S in 1 M KCl, and (D) 20 wt % NaXS in 1 M KCl. The best-fit simulation parameters are provided in Table S2.

https://doi.org/10.1021/acsomega.1c05133
ACS Omega 2021, 6, 30800−30810

Table 1. Calculated D_{red}, D_{ox}, and k^0 Values for 4-OH-TEMPO Collected from CV, LSV, and EIS Experiments[a]

	D_{red} [cm^2/s]		D_{ox} [cm^2/s]		k^0 [cm/s]		
electrolyte	CV	LSV	CV	LSV	CV	LSV	EIS
1 M KCl	$7.00 \pm 0.24 \times 10^{-6}$	10.53×10^{-6}	$6.82 \pm 0.32 \times 10^{-6}$	6.03×10^{-6}	0.35 ± 0.14	0.09 ± 0.07	0.08 ± 0.00
20 wt % NaXS	$3.33 \pm 0.04 \times 10^{-6}$	6.63×10^{-6}	$3.50 \pm 0.11 \times 10^{-6}$	3.76×10^{-6}	0.48 ± 0.19	0.12 ± 0.11	0.29 ± 0.11
20 wt % Na*p*TS	$4.27 \pm 0.14 \times 10^{-6}$	8.53×10^{-6}	$4.92 \pm 0.15 \times 10^{-6}$	4.40×10^{-6}	0.95 ± 0.07	0.32 ± 0.33	0.12 ± 0.01
20 wt % urea	$5.90 \pm 0.07 \times 10^{-6}$		$5.55 \pm 0.12 \times 10^{-6}$		0.78 ± 0.16		

[a]The CV experiments were conducted with an initial 4-OH-TEMPO concentration of 1 mM. The LSV and EIS experiments were conducted with 1 mM 4-OH-TEMPO and 1 mM-oxidized 4-OH-TEMPO radical. The solutions contained 1 M KCl, 20 wt % NaXS in 1 M KCl, 20 wt % NapTS in 1 M KCl, or 20 wt % urea in 1 M KCl.

experiments over rotating disk electrode experiments was that CV measurements could be made with far smaller sample volumes.

We confirmed that the diffusion coefficient for 4-OH-TEMPO (D_{red}) was moderately larger in the absence of a hydrotrope ($7.00 \pm 0.24 \times 10^{-6}$ cm^2/s) than in cases in which 20 wt % hydrotrope was present (NaXS: $3.33 \pm 0.04 \times 10^{-6}$ cm^2/s, Na*p*TS: $4.27 \pm 0.14 \times 10^{-6}$ cm^2/s, urea: $5.90 \pm 0.07 \times 10^{-6}$ cm^2/s) from CV fitting results (Table 1). We observed the same trend of D_{red} values decreasing in the presence of a hydrotrope in the LSV data, although the absolute D_{red} values were all calculated to be slightly higher (no hydrotrope: 10.53×10^{-6} cm^2/s, NaXS: 6.63×10^{-6} cm^2/s, Na*p*TS: 8.53×10^{-6} cm^2/s, Table 1). The D_{red} values measured in the absence of a hydrotrope (CV: $7.00 \pm 0.24 \times 10^{-6}$ cm^2/s, LSV: 10.53×10^{-6} cm^2/s) both agree well with previously reported values in aqueous solutions (7.7×10^{-6},[42] 11.5×10^{-6},[43] 29.5×10^{-6} cm^2/s[11]). The diffusion coefficients for the oxidized 4-OH-TEMPO radical (D_{ox}) were calculated to be slightly smaller or approximately the same as the D_{red} values for each of the solutions tested (Table 1). There were not any significant differences between the $E^{0'}$ or the transfer coefficient (α) values fitted from the CVs in the absence or presence of a hydrotrope (Table S2).

The observation that the presence of a hydrotrope decreased D_{red} values was likely a consequence of hydrotropes increasing the solution viscosity, as opposed to the hydrotrope actively altering the mobility of 4-OH-TEMPO. According to the Stokes–Einstein equation, which describes the movement of spherical particles, diffusion coefficients are inversely proportional to the solution viscosity

$$D = \frac{k_b T}{6\pi\mu r} \quad (1)$$

where k_b is the Boltzmann constant, T is the thermodynamic temperature, μ is the dynamic viscosity of the solution, and r is the molecular radius. We measured the viscosities of each solution in the absence of a hydrotrope (9.1×10^{-4} Pa·s) and in the presence of 20 wt % NaXS (1.8×10^{-3} Pa·s) or Na*p*TS: (1.9×10^{-3} Pa·s). Using these values, we calculated the hydraulic radius of 4-OH-TEMPO based on D_{red} from the CV data, μ, and T (298K) for the three solutions. The calculated hydraulic radii of 4-OH-TEMPO were similar for all of the solutions (no hydrotrope: 3.3 Å, NaXS: 3.7 Å, Na*p*TS: 2.7 Å), indicating that the hydrotrope did not actively alter the hydrated radius of 4-OH-TEMPO via molecular interactions.

We quantified k^0 values for 4-OH-TEMPO in each of the solutions by fitting the CV data collected with a glassy carbon electrode (Table 1). The data generally showed that the presence of a hydrotrope slightly increased the k^0 values, although the differences were near the experimental errors. For a subset of the experimental conditions, we also quantified k^0 values using the LSV data (Figures S3 and S4)[44] and EIS measurements (Figure S5). The k^0 values agreed well among the techniques, with the CV values being slightly larger than those obtained with the other two techniques (Table 1). The k^0 value measured in the absence of a hydrotrope (CV value: 0.35 ± 0.14 cm/s) was approximately an order of magnitude higher than a previously reported value measured in an aqueous electrolyte using a glassy carbon working electrode (0.0157 cm/s).[43] The reason for the discrepancy among the values measured here and the value reported in the previous study remains unclear.

No previous studies have examined how hydrotropes influence k^0 values, but insights can be gained from comparing the observations reported here and the previous studies examining the effects that surfactants have on k^0 values. In contrast to our observations, surfactants can have a large impact on k^0 values, with changes scaling up to 2 orders of magnitude in either direction.[45] In the case of the surfactants, the direction and scale of the effect appear to depend both on the nature and strength of electrostatic and hydrophobic interactions between the surfactant and solute.[45−48] The lack of a substantial change in k^0 values observed here suggests that 4-OH-TEMPO does not strongly interact with the hydrotropes studied, consistent with the hydrotropes having a minimal impact D or $E^{0'}$ values.

Influence of Hydrotrope on BDS. We characterized the electrochemical properties of BDS (Figure 5A) in the presence of the hydrotrope proline to determine if the trends observed for 4-OH-TEMPO also applied to another hydrotrope redox-active compound combination. BDS coupled with hydrotrope proline yielded the largest solubility increase in BDS (Figure 2E). The compound BDS is known to undergo a two-electron-transfer reaction in acidic solutions (Figure 5B).[29,49] The cyclic voltammograms collected in the presence and absence of proline demonstrated that proline did not alter $E^{0'}$ (0.71 ± 0.01 V vs Ag/AgCl for both solutions, Figure 5B), indicating that proline did not preferentially alter the solvation energies (ΔG^0_{solv}) of the reduced or oxidized forms of BDS.[40] In a control CV experiment lacking the redox-active compound BDS, we confirmed that proline itself did not undergo any electron-transfer reaction (Figure S2). Note the $E^{0'}$ value measured here in 1 M H_2SO_4 (0.70 V vs Ag/AgCl) was slightly higher than a previously reported $E^{0'}$ value (0.64 V vs Ag/AgCl) measured in 1 M H_2SO_4.[29,49] The CVs collected at a scan rate of 10 mV/s showed a quasi-reversible current response with large peak separations (*peak separation*: no hydrotrope: 251 mV, proline: 257 mV), indicating that k^0 was

https://doi.org/10.1021/acsomega.1c05133
ACS Omega 2021, 6, 30800−30810

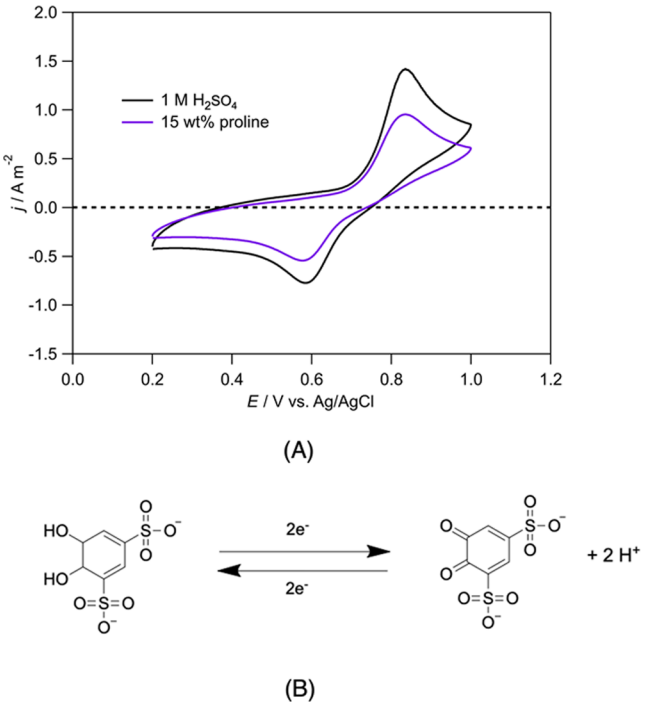

Figure 5. (A) Cyclic voltammetry of 1 mM 4,5-dihydroxy-1,3-benzenedisulfonate (BDS) in 1 M H_2SO_4 and 1 M H_2SO_4 with 15 wt % proline. v = 10 mV/s. (B) Half-reaction of BDS.

not sufficiently large relative to D_{ox} and D_{red} values to achieve fully reversible electron-transfer kinetics.[41] The high-peak separation value aligned with a literature reported value at the same scan rate (280 mV).[49] The decreases in the peak current heights in the presence of a hydrotrope also suggested that the hydrotrope decreased both D_{ox} and D_{red} values.

We used the same approach as for 4-OH-TEMPO, in which we simultaneously fit cyclic voltammograms collected at several scan rates to determine D values for BDS in the presence and absence of proline (Figure 6). The diffusion coefficient for BDS (D_{red}) in the absence of a hydrotrope (3.85 ± 0.21 × 10^{-6} cm^2/s) was larger than the value in 15 wt % proline (1.97 ± 0.04 × 10^{-6} cm^2/s) (Table 2). The LSV data corroborated this trend, although D_{red} values were approximately twice as large when calculated from LSV data (no hydrotrope: $D_{red,LSV}$: 4.88 × 10^{-6} cm^2/s, proline: $D_{red,LSV}$: 2.33 × 10^{-6} cm^2/s) (Table 2). In addition, we observed in the CV simulation results that in both solutions, D_{ox} was smaller than D_{red}. The difference between BDS's D_{red} and D_{ox} was reflected on the voltammograms' peak currents in each scan direction, where the peak current in the oxidation side was higher than the value of the peak current in the reduction side (Figure 5A). When fitting CV curves, we tested if a chemical degradation reaction of oxidized BDS caused the lower peak current during reduction relative to the oxidation peak, but adding a chemical reaction to the model did not improve the quality of the fit or the fitted electrochemical parameters (Figure S6, Table S3). The D_{red} values we measured in 1 M H_2SO_4 ($D_{red,CV}$: 3.85 ± 0.21 × 10^{-6} cm^2/s, $D_{red,LSV}$: 4.88 × 10^{-6} cm^2/s) were both comparable to previously reported values in 1 M H_2SO_4 (5.1 × 10^{-6},[49] 3.8 × 10^{-6} cm^2/s[13]). We did not observe a significant difference between the $E^{0'}$ and α value from the fitting results with and without the presence of a hydrotrope (Table S3). We confirmed that the reason D decreased in the presence of the hydrotrope was most likely a consequence of proline increasing the solution viscosity, as the radii of BDS in both solutions calculated with eq 1 were approximately equal (no hydrotrope: 5.8 Å, proline: 6.6 Å).

We quantified k^0 values for BDS using the CV and LSV data (Table 2, Figures S7 and S8). The CV data yielded the similar k^0 values in the presence and the absence of proline (no hydrotrope: 1.73 ± 0.10 × 10^{-5} cm/s, 15 wt % proline: 2.06 ± 0.07 × 10^{-5} cm/s; Table 2), while from our LSV experiment, BDS's k^0 was found to decrease from 20.4 ± 8.5 × 10^{-5} cm/s in the absence of a hydrotrope to 9.8 ± 3.6 × 10^{-5} cm/s in 15 wt % proline. The reaction rate constant value reported for quinone compounds in 1 M H_2SO_4 was in the range of 10^{-3}–10^{-4} cm/s,[13,29] which was close to our calculated heterogeneous rate constant (k_h) value of BDS in the absence of a hydrotrope from the LSV data (1.52 ± 0.46 × 10^{-4} cm/s). Collectively, the data indicated that proline slightly decreased k^0 on a glassy carbon electrode.

Implications for Flow Batteries. The solubility experiments indicated that hydrotropes can increase the solubilities of redox-active compounds relevant to aqueous redox flow batteries. There was not a general trend in how each hydrotrope influenced the solubilities of the redox-active compounds, as each compound–hydrotrope combination yielded different degree of solubility change, consistent with past studies examining the solubilization of organic compounds using hydrotropes.[27,33−37] We successfully demonstrated that the hydrotrope NaXS could increase the solubility of 4-OH-TEMPO by 69%, indicating that the theoretical energy storage density of the aqueous redox flow battery using 4-OH-TEMPO as the electroactive species could be significantly improved. Our electrochemical data indicated that for 4-OH-TEMPO and BDS, the addition of a hydrotrope slightly decreased both D_{ox} and D_{red} values, which was likely caused by the hydrotropes

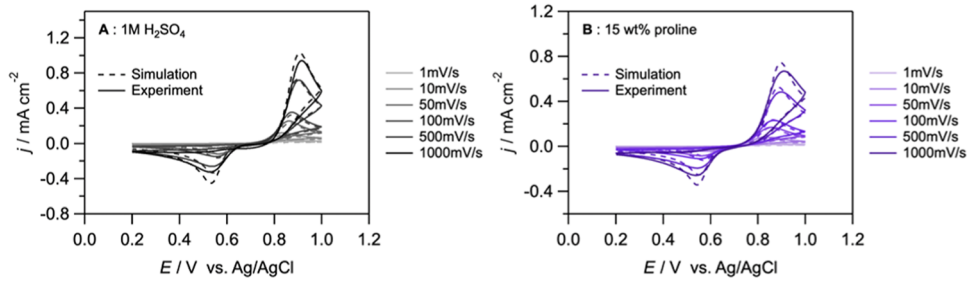

Figure 6. CV simulation and experiment result of 1 mM BDS in (A) 1 M H_2SO_4 and (B) 15 wt % proline in 1 M H_2SO_4.

https://doi.org/10.1021/acsomega.1c05133
ACS Omega 2021, 6, 30800−30810

Table 2. CV Simulation Fitting Results of 1 mM BDS in 1 M H_2SO_4 and 15 wt % Proline Solutions[a]

	D_{red} [cm^2/s]		D_{ox} [cm^2/s]		k^0 [cm/s]	
electrolyte	CV	LSV	CV	LSV	CV	LSV
1 M H_2SO_4	$3.85 \pm 0.21 \times 10^{-6}$	4.88×10^{-6}	$3.67 \pm 0.86 \times 10^{-6}$		$1.73 \pm 0.10 \times 10^{-5}$	$20.42 \pm 8.53 \times 10^{-5}$
15 wt % proline	$1.97 \pm 0.04 \times 10^{-6}$	2.33×10^{-6}	$2.94 \pm 0.15 \times 10^{-6}$		$2.06 \pm 0.07 \times 10^{-5}$	$9.84 \pm 3.63 \times 10^{-5}$

[a]LSV fitting results of 2 mM BDS in 1 M H_2SO_4 and 15 wt % proline solutions in 1 M H_2SO_4.

increasing solution viscosities. With respect to k^0, 4-OH-TEMPO's value slightly increased in the presence of hydrotropes, while the BDS's value slightly decreased. Compared to molecular modification techniques, amending the solution with hydrotropes had less of an effect on a redox-active compound solubility,[50] but it offered an alternative means for achieving solubility changes without substantially altering the reactivities of the compound. On a practical level, the presence of a hydrotrope will increase the solution viscosity, which would increase pumping costs in a flow battery.

EXPERIMENTAL SECTION

Chemicals. All of the chemicals used were used without further purification. The five redox-active organic molecules studied were 4-OH-TEMPO free radical (>98%, Alfa Aesar), methyl viologen (98%, Acros Organics), riboflavin-5′-monophosphate (>93%, Tokyo Chemical Industry Co.), anthraquinone-2,7-disulfonate (>97%, Tokyo Chemical Industry Co.), and 4,5-dihydroxy-1,3-benzenedisulfonate (97%, Sigma-Aldrich). The five hydrotropes used were proline (99%, Alfa Aesar), sodium xylenesulfonate (NaXS) (<9.0% sodium sulfate, Sigma-Aldrich), sodium *para*-toluenesulfonate (Na*p*TS) (99%, Spectrum), urea (GR for analysis, Sigma-Aldrich), and *tert*-butanol (TBA) (≥99.0%, Sigma-Aldrich). We electrochemically oxidized 4-OH-TEMPO radical ($E^{0'}$ = 0.59 V vs Ag/AgCl) to 4-OH-TEMPO$^+$ for use in electrochemical tests with a custom-made glassy carbon bulk electrolysis cell by applying a potential of 0.75 V vs Ag/AgCl (MF-2056, BASi) for 5−10 h, depending on the solution concentration. The conversion of 4-OH-TEMPO radical to 4-OH-TEMPO$^+$ was monitored by stopping the electrochemical oxidation reaction once per hour and measuring the open-circuit potential. It was stopped when the open-circuit potential reached 0.72 V vs Ag/AgCl, which indicated that 99% of the 4-OH-TEMPO radical in the solution had been converted to 4-OH-TEMPO$^+$ according to the Nernst equation

$$E = E^0 - \frac{RT}{nF} \ln Q \tag{2}$$

where E is the cell potential, E^0 is the formal reduction potential, R is the universal gas constant, n is the number of electrons transferred, F is the Faraday constant, T is the temperature, and Q is the reaction quotient (in this case: $\frac{4-OH-TEMPO}{4-OH-TEMPO^+}$).

Solubility Measurements. All experiments were conducted with deionized water having a resistivity >18 MΩ·cm. The solubility experiments were all performed in triplicate, with reported errors representing the standard deviations among them. The hydrotropic solvents were made gravimetrically by combining the hydrotrope salt or liquid with 1 M KCl, 1 M H_2SO_4, or 1 M KOH, depending on the organic compounds used. The maximum hydrotrope weight percentage was limited to 20 wt % because in the preliminary experiments, we observed phase separations when using higher hydrotrope concentrations and 1 M KCl. All hydrotrope solutions were equilibrated at least 24 h prior to the solubility experiments. After equilibration, an excess of a redox-active compound was added, allowed the solutions to equilibrate for at least 24 h, and then measured the concentration. The solubility tests on AQDS were not performed with the hydrotrope urea or TBA because we ran out of 97% purity AQDS compounds, and it was no longer commercially available.

The solubilities of each organic compound in each solution were measured using UV−vis spectroscopy (PerkimElmer Lambda35 UV−vis Spectrophotometer; UV-1800, Shimadzu USA MFG INC.). The PerkimElmer Lambda35 UV−vis was used for experiments with NaXS, Na*p*TS, and proline, and the UV-1800 instrument was used for experiments with urea and TBA. The reason for the switch between instruments was that the Lambda35 stopped working over the course of the experiments. For all solubility measurements, a small volume (∼10 μL) from the top layer of each saturated solution without any visible undissolved suspended solids presented was taken, then got diluted 10 000-fold with DI water prior to measurements to decrease the absorbance to a value within our standard curves. For a subset of the solutions, the initial sample was filtered through a 0.2 μm PTFE syringe filter prior to the dilution step to rule out the possibility that the samples contained suspended particulate material. Filtering the samples had a negligible effect on the measured solubility values. The dilution step decreased the hydrotrope concentration in our measured solutions, which was important because some hydrotropes had overlapping absorbances with some of the redox-active compounds. No hydrotrope peaks were present in the UV−vis spectra in control measurements lacking the redox-active compounds. The wavelengths used to record peak absorbances for each compound were as follows: MeV: 258 nm, 4-OH-TEMPO: 243 nm, AQDS: 328 nm, BDS: 291 nm, and FMN: 446 nm. The molar attenuation coefficient for each compound was calculated from our standard curves using the Beer−Lambert Law (MeV: $1.35 \pm 0.17 \times 10^3$ m^2/mol, 4-OH-TEMPO: $2.45 \pm 0.10 \times 10^2$ m^2/mol, AQDS: $6.04 \pm 0.21 \times 10^2$ m^2/mol, BDS: $3.50 \pm 0.33 \times 10^2$ m^2/mol, and FMN: $7.30 \pm 0.85 \times 10^2$ m^2/mol).[51] The calibration curves for each compound are provided in the Supporting Information (Figure S9).

Cyclic Voltammetry. Cyclic voltammetry experiments were conducted using a CH Instruments potentiostat (model 630E) in a three-electrode cell containing a glassy carbon working electrode (BASi MF-2012, 3 mm diameter, area = 0.0707 cm^2), an Ag/AgCl reference electrode in 3 M KCl (BASi MF-2056), and a platinum wire counter electrode. Before each experiment, the working electrode was polished with 0.05 μm of alumina particles on the microcloth pad and then rinsed with DI water and methanol. For 4-OH-TEMPO, the pH of all electrolytes containing a hydrotrope was

https://doi.org/10.1021/acsomega.1c05133
ACS Omega 2021, 6, 30800−30810

readjusted to pH = 7.0 using 1 M HCl solution. For BDS, the pH of the electrolytes containing a hydrotrope was readjusted to ~0 using 2.5 M H_2SO_4. For each organic compound, the triplicate CVs were collected in scan rates of 0.001, 0.01, 0.05, 0.1, 0.5, and 1 V/s. For each scan rate, three cycles of CV data were collected. The CV data without the redox-active organic compound in otherwise identical electrolytes using the same scan rates were also collected to subtract out the background capacitive current from data.

A finite-element model describing the reactions during cyclic voltammetry was created using the method described in Bard and Faulkner.[41] 1D finite-element analysis was used with uniform space (Δx) and time (Δt) discretization to solve the concentrations of the oxidized (c_o) and reduced (c_r) species as functions of time and distance from the electrode. The concentrations followed Fick's second law of diffusion in one dimension

$$\frac{dc_m(x,t)}{dt} = D_m \frac{d^2c_m(x,t)}{dx^2} \tag{3}$$

where D_m is the diffusion coefficient of species m. For the boundary condition farthest from the electrode, $x_{n,max}$, we held the concentration constant at the starting bulk concentration; we modeled a sufficiently large distance from the electrode (>0.5 cm) such that this boundary condition had no impact on the simulated voltammograms. For the electrode boundary condition, x_0, the electrochemical reactions at the electrode surface were modeled as first-order reactions. The rate constants for the forward (reduction) reaction and backward (oxidation) reaction, k_f and k_b, respectively, were defined as in the Butler–Volmer equation

$$k_f(t) = k^0 \exp(-\alpha (E(t) - E^{0'})nF) \tag{4}$$

$$k_b(t) = k^0 \exp((1-\alpha)(E(t) - E^{0'})nF) \tag{5}$$

where k^0 is the electrochemical rate constant (cm/s), α is the unitless charge-transfer coefficient, n is the number of electrons transferred, $E(t)$ is the electrode potential at time t, $E^{0'}$ is the formal reduction potential, and F is Faraday's constant. We solved Fick's first law of diffusion to obtain the flux of species m at the surface, $J_m(t)$

$$J_m(t) = -D_m \frac{dc_m(x = x_0, t)}{dx} \tag{6}$$

Given the flux of the oxidized species at the electrode, the current due to the electrochemical reaction $\hat{i}(t)$ was defined by Faraday's law of electrolysis

$$\frac{\hat{i}(t)}{A} = -nFJ_o(t) \tag{7}$$

The CV simulation was written as a function with the following inputs: the diffusion coefficients of the oxidized and reduced species (D_o, D_r), $E^{0'}$, k^0, α, uniformly spaced $E(t)$, scan rate (ν), and total concentration. It was assumed that for a voltammogram that started with an increasing electrode potential, the starting concentration of the reduced species for all space was equal to the total concentration. The simulation then solved the set of differential equations to return the current density (mA/cm^2) for three consecutive cycles. The third cyclic voltammogram was compared to the experimentally collected third scan of the cyclic voltammogram after background subtracting the capacitive current that was experimentally measured under identical conditions.

The simulation was regressed through repeated cycles to find the values of D_o, D_r, $E^{0'}$, k^0, and α whose simulation current, $\hat{i}(t)$, best fit the background-subtracted experimental current, $i(t)$, data. The data were fitted for all scan rates simultaneously using a single objective function. The best-fit values for D_o, D_r, $E^{0'}$, k^0, and α were those that minimized the weighted sum of a squares error function, WSSE

$$\text{WSSE} = \sum_{j \in \text{dataset}} (\hat{i}(t_j) - i(t_j))^2 * w(t_j) \tag{8}$$

where the weight, w, at time t_j was defined as the following

$$w(t_j) = \max_{\nu_k=\nu_j}(|i(t_k)|)^{-1} * \frac{d^2i(t_j)}{dE^2} \max_{\nu_k=\nu_j}\left(\left|\frac{d^2i(t_k)}{dE^2}\right|\right)^{-1} \tag{9}$$

In eq 9, $\max_{\nu_k=\nu_j}(X(t_k))$ refers to the maximum value of variable X among the set of time points t_k that have the same scan rate as the point t_j. For example, if t_j was obtained from a CV with a scan rate 0.05 V/s, $\max_{\nu_k=\nu_j}(|i(t_k)|)$ would be the maximum absolute value of the current from that CV. Conceptually, this weighting function is the product of (a) the inverse of the absolute value of maximum current obtained for that scan rate and (b) the normalized second derivative of current with respect to voltage at that time point. Part a of the weighting factor accounts for the increase in the current magnitudes with the scan rate, preventing it from overprioritizing the quality of fit to higher scan rates, where the same percent error yields a larger sum of squares error. Part b of the weighting factor prioritizes the quality of fit to the peaks in the voltammogram, which are the most characteristic features in a CV with a Faradaic reaction. The second derivative at a given time index j is approximated by fitting the 15 points around it in the same scan direction $\{j-7, j-6, ..., j+7\}$ to a parabola and taking the second derivative of the parabola. The WSSE objective function was minimized using a genetic algorithm (GA package v.3.2 in R v.4.0.3).[52,53] Convergence was defined as 20 generations where the minimum value is unchanged or after a maximum of 80 generations.

The uncertainties of fitting parameters were approximated using a jack-knifing method that treated each scan rate as an independent sample. Instead of regressing the simulation to the entire data set, we regressed it to the partial data set, where one scan rate was removed. This was repeated for all possible partial data sets in which only one scan rate was removed, producing a set of fitting parameters. The standard deviation of this set of fitting parameters was treated as an estimate for the standard error of the best fit.[54]

For BDS, the simulation was adjusted to include a term for the decomposition of the oxidized species to determine if including degradation improved the model's quality of fit. The degradation was modeled as a first-order reaction

$$c_o^*(x_n, t + \Delta t) = c_o(x_n, t + \Delta t) - \frac{k_d}{\Delta t} c_o(x_n, t) \tag{10}$$

where $c_o^*(x,t)$ is the modified value of the concentration in the absence of a reaction, $c_o(x,t)$, to include the spontaneous reaction. In these trials, including this term did not significantly improve the quality of the fits and did not significantly change

https://doi.org/10.1021/acsomega.1c05133
ACS Omega 2021, 6, 30800−30810

the values for D_o, D_r, $E^{0'}$, k^0, α, so we did not include it in the reported best-fit parameters.

Electrochemical Impedance Spectroscopy and Linear Sweep Voltammetry. Electrochemical impedance spectroscopy (EIS) and linear sweep voltammetry (LSV) experiments were conducted with Gamry potentiostat (REF 600P) in a three-electrode cell: a glassy carbon rotation disk electrode (5 mm diameter Teflon-encased glassy carbon disk, Pine Research Instrument), a Ag/AgCl reference electrode (MF-2056, BASi), and a platinum wire counter electrode. Before each experiment, the electrode was polished using the same protocol as described for cyclic voltammetry experiments. For EIS and LSV experiments with 4-OH-TEMPO, the solutions used were 1 mM radical 4-OH-TEMPO and 1 mM 4-OH-TEMPO$^+$ dissolved in 1 M KCl, 20 wt % NaXS, or 20 wt % Na*p*TS. The known concentrations of both 4-OH-TEMPO species facilitated the calculation of exchange current density

$$R_{ct} = \frac{RT}{nFj_0} \tag{11}$$

where R_{ct} is the charge-transfer resistance in Ω and j_0 is the exchange current density in A/cm^2 (electrode area: 0.196 cm^2). The EIS experiment for 4-OH-TEMPO was conducted in an open-circuit potential, with a rotation rate of 2500 rpm, an amplitude of 10 mV, and frequencies between 0.5 and 100 000 Hz. The Nyquist plot was fitted using Electrochemical Impedance Spectroscopy Software from Gamry to quantify R_{ct}, which was then used to calculate j_0 according to eq 11. Then, j_0 was used to calculate the electrochemical rate constant (k^0) assuming that α was 0.5 (note that the α values from our CV simulation results were close to 0.5; Tables S3 and S4)

$$j_0 = Fk^0(C_{ox}^{1-\alpha}C_{red}^{\alpha}) \tag{12}$$

The LSV experiments for 4-OH-TEMPO were carried out at a scan rate of 10 mV/s, and the electrode was rotated at 1500, 1750, 2000, 2250, and 2500 rotations per minute (rpm). The cutoff voltages were set to 0.3 and 0.9 V vs Ag/AgCl. The oxidizing and reducing limiting currents were measured at 0.88 and 0.30 V, respectively. The kinetically dominated currents were selected at overpotentials than 0.05 V. Both the limiting current and the kinetically dominated current were fitted against reciprocal of the square root of rotation rate (rad/s) according to the Koutecky–Levich equation[44]

$$\frac{1}{I} = \frac{1}{0.62nF\pi r^2 D^{2/3}\nu^{-1/6}\omega^{1/2}C} + \frac{1}{nF\pi r^2 k_h C} \tag{13}$$

where D is the diffusion coefficient, ν is the kinematic viscosity, C is the bulk concentration, ω is the rotation rate, η is the overpotential, and k_h is the heterogeneous rate constant for electron transfer, defined as

$$k_h = k^0 \exp[\frac{-\alpha F\eta}{RT}] \tag{14}$$

The first half of eq 13 describes the mass transfer dominated limiting currents, and the second half describes the kinetically dominated (cathodic and anodic) currents. The current was fitted using eq 13 to yield a linear plot, with the slope of $\frac{1}{0.62nF\pi r^2 D^{2/3}\nu^{-1/6}C}$ and intercept of $\frac{1}{nF\pi r^2 k_h C}$, where r was 0.25 mm. By fitting limiting currents and kinetically dominated currents against the reciprocal of the square root of the rotation rate, D and k_h values of both radical 4-OH-TEMPO and 4-OH-TEMPO$^+$ were calculated from the slope and intercept values.

For BDS, LSV experiments were conducted using solutions containing 2 mM BDS in 1 M H_2SO_4 and 15 wt % proline. The rotation rates applied for BDS's LSV experiments were 500, 750, 1000, 1250, and 1500 rpm. Because the solution started with only the reduced species, we only recorded oxidizing limiting currents at 1.15 V and kinetically dominated anodic currents at overpotential <0.05 V. The diffusion coefficient of reduced BDS species was calculated using eq 13 using the same approach as described above for 4-OH-TEMPO.

Viscosity Measurements. The viscosities of 1 M KCl, 20 wt % NaXS, and 20 wt % Na*p*TS were measured using a rotational rheometer (RFS3) with concentric cylinder geometry with a shear rate from 10 to 100/s (Table S4). The viscosities of 1 M H_2SO_4 and 15 wt % proline were measured using a Ubbelohde glass viscometer (CUC-50 CANNON-Ubbelohde calibrated) (Table S4).

■ ASSOCIATED CONTENT

Supporting Information

The Supporting Information is available free of charge at https://pubs.acs.org/doi/10.1021/acsomega.1c05133.

The comparison of solubilities of redox-active compounds from our experimental measurements and reference values in the literature; the aqueous solubilities of redox-active compounds as a function of hydrotrope concentration in molarity; cyclic voltammograms for background electrolytes without the redox-active organic compound; the fitting results of 4-OH-TEMPO CVs; linear sweep voltammograms of 1 mM 4-OH-TEMPO-(+) and 1 mM 4-OH-TEMPO(•); Koutecký–Levich plots for 1 mM 4-OH-TEMPO(+) and 1 mM 4-OH-TEMPO(•); Nyquist plots from EIS measurements; comparison of CV simulation results with and without the chemical degradation parameter; the fitting results of BDS CVs; linear sweep voltammograms of 2 mM 4,5-dihydroxy-1,3-benzenedisulfonate (BDS); Koutecký–Levich plots for 2 mM BDS; calibration curves (UV–vis absorbance versus concentration) for the five redox-active organic compounds; and the hydrodynamic viscosity measurements of 1 M KCl, 20 wt % NaXS, and 20 wt % Na*p*TS, 1 M H_2SO_4, and 15 wt % proline (PDF)

■ AUTHOR INFORMATION

Corresponding Author

Christopher A. Gorski − *Department of Civil and Environmental Engineering, Pennsylvania State University, University Park, Pennsylvania 16802, United States;* orcid.org/0000-0002-5363-2904; Phone: (814) 865-5673; Email: gorski@psu.edu

Authors

Yingchi Cheng − *Department of Civil and Environmental Engineering, Pennsylvania State University, University Park, Pennsylvania 16802, United States*

Derek M. Hall − *Department of Energy and Mineral Engineering and Earth and Mineral Sciences Energy Institute, Pennsylvania State University, University Park, Pennsylvania 16802, United States;* orcid.org/0000-0001-9648-596X

Jonathan Boualavong − *Department of Civil and Environmental Engineering, Pennsylvania State University, University Park, Pennsylvania 16802, United States*

Robert J. Hickey − *Department of Material Sciences and Engineering, Pennsylvania State University, University Park, Pennsylvania 16802, United States;* orcid.org/0000-0001-6808-7411

Serguei N. Lvov − *Department of Energy and Mineral Engineering, Earth and Mineral Sciences Energy Institute, and Department of Material Sciences and Engineering, Pennsylvania State University, University Park, Pennsylvania 16802, United States*

Complete contact information is available at: https://pubs.acs.org/10.1021/acsomega.1c05133

Notes

The authors declare no competing financial interest.

■ ACKNOWLEDGMENTS

The authors acknowledge the financial support for this research from Penn State University SEED Grant program and National Science Foundation Grant no. CBET-1603635. The authors thank Aijie Han's assistance of the viscosity measurements for NaXS, Nap*T*S, and proline's solution.

■ REFERENCES

(1) Wang, W.; Luo, Q.; Li, B.; Wei, X.; Li, L.; Yang, Z. Recent Progress in Redox Flow Battery Research and Development. *Adv. Funct. Mater.* **2013**, *23*, 970−986.

(2) Crawford, A.; Viswanathan, V.; Stephenson, D.; Wang, W.; Thomsen, E.; Reed, D.; Li, B.; Balducci, P.; Kintner-Meyer, M.; Sprenkle, V. Comparative Analysis for Various Redox Flow Batteries Chemistries Using a Cost Performance Model. *J. Power Sources* **2015**, *293*, 388−399.

(3) Nourai, A. In *Large-Scale Electricity Storage Technologies for Energy Management*, Proceedings of IEEE Power Engineering Society Transmission and Distribution Conference, 2002; pp 310−315.

(4) Soloveichik, G. L. Flow Batteries: Current Status and Trends. *Chem. Rev.* **2015**, *115*, 11533−11558.

(5) Perry, M. L.; Weber, A. Z. Advanced Redox-Flow Batteries: A Perspective. *J. Electrochem. Soc.* **2016**, *163*, A5064−A5067.

(6) Bachman, J. E.; Curtiss, L. A.; Assary, R. S. Investigation of the Redox Chemistry of Anthraquinone Derivatives Using Density Functional Theory. *J. Phys. Chem. A* **2014**, *118*, 8852−8860.

(7) Leung, P.; Shah, A. A.; Sanz, L.; Flox, C.; Morante, J. R.; Xu, Q.; Mohamed, M. R.; Ponce de León, C.; Walsh, F. C. Recent Developments in Organic Redox Flow Batteries: A Critical Review. *J. Power Sources* **2017**, *360*, 243−283.

(8) Li, B.; Liu, J. Progress and Directions in Low-Cost Redox-Flow Batteries for Large-Scale Energy Storage. *Natl. Sci. Rev.* **2017**, *4*, 91−105.

(9) Li, Z.; Lu, Y. C. Redox Flow Batteries: Want More Electrons? Go Organic! *Chem* **2018**, *4*, 2020−2021.

(10) Yang, B.; Hoober-Burkhardt, L.; Wang, F.; Surya Prakash, G. K.; Narayanan, S. R. An Inexpensive Aqueous Flow Battery for Large-Scale Electrical Energy Storage Based on Water-Soluble Organic Redox Couples. *J. Electrochem. Soc.* **2014**, *161*, A1371−A1380.

(11) Liu, T.; Wei, X.; Nie, Z.; Sprenkle, V.; Wang, W. A Total Organic Aqueous Redox Flow Battery Employing a Low Cost and Sustainable Methyl Viologen Anolyte and 4-HO-TEMPO Catholyte. *Adv. Energy Mater.* **2015**, *6*, No. 1501449.

(12) Huskinson, B.; Marshak, M. P.; Suh, C.; Er, S.; Gerhardt, M. R.; Galvin, C. J.; Chen, X.; Aspuru-Guzik, A.; Gordon, R. G.; Aziz, M. J. A Metal-Free Organic-Inorganic Aqueous Flow Battery. *Nature* **2014**, *505*, 195−198.

(13) Yang, B.; Hoober-Burkhardt, L.; Wang, F.; Prakash, G. K. S.; Narayanan, S. R. An Inexpensive Aqueous Flow Battery for Large-Scale Electrical Energy Storage Based Onwater-Soluble Organic Redox Couples. *J. Electrochem. Soc.* **2014**, *161*, A1371.

(14) Wedege, K.; Dražević, E.; Konya, D.; Bentien, A. Organic Redox Species in Aqueous Flow Batteries: Redox Potentials, Chemical Stability and Solubility. *Sci. Rep.* **2016**, *6*, No. 39101.

(15) Ding, Y.; Zhang, C.; Zhang, L.; Wei, H.; Li, Y.; Yu, G. Insights into Hydrotropic Solubilization for Hybrid Ion Redox Flow Batteries. *ACS Energy Lett.* **2018**, *3*, 2641−2648.

(16) Orita, A.; Verde, M. G.; Sakai, M.; Meng, Y. S. A Biomimetic Redox Flow Battery Based on Flavin Mononucleotide. *Nat. Commun.* **2016**, *7*, No. 13230.

(17) Ding, Y.; Yu, G. Molecular Engineering Enables Better Organic Flow Batteries. *Chem* **2017**, *3*, 917−919.

(18) DeBruler, C.; Hu, B.; Moss, J.; Liu, X.; Luo, J.; Sun, Y.; Liu, T. L. Designer Two-Electron Storage Viologen Anolyte Materials for Neutral Aqueous Organic Redox Flow Batteries. *Chem* **2017**, *3*, 961−978.

(19) Schwan, S.; Schröder, D.; Wegner, H. A.; Janek, J.; Mollenhauer, D. Substituent Pattern Effects on the Redox Potentials of Quinone-Based Active Materials for Aqueous Redox Flow Batteries. *ChemSusChem* **2020**, *13*, 5480−5488.

(20) Er, S.; Suh, C.; Marshak, M. P.; Aspuru-Guzik, A. Computational Design of Molecules for an All-Quinone Redox Flow Battery. *Chem. Sci.* **2015**, *6*, 885−893.

(21) Luo, J.; Hu, B.; Debruler, C.; Liu, T. L. A π-Conjugation Extended Viologen as a Two-Electron Storage Anolyte for Total Organic Aqueous Redox Flow Batteries. *Angew. Chem. Int. Ed.* **2018**, *57*, 231−235.

(22) Hodgdon, T. K.; Kaler, E. W. Hydrotropic Solutions. *Curr. Opin. Colloid Interface Sci.* **2007**, *12*, 121−128.

(23) Shimizu, S.; Nagai, Y. Effect of Solute Aggregation on Solubilization. *J. Mol. Liq.* **2019**, *274*, 209−214.

(24) Booth, J. J.; Abbott, S.; Shimizu, S. Mechanism of Hydrophobic Drug Solubilization by Small Molecule Hydrotropes. *J. Phys. Chem. B* **2012**, *116*, 14915−14921.

(25) Srinivas, V.; Rodley, G. A.; Ravikumar, K.; Robinson, W. T.; Turnbull, M. M. Molecular Organization in Hydrotrope Assemblies. *Langmuir* **1997**, *13*, 3235−3239.

(26) Hopkins Hatzopoulos, M.; Eastoe, J.; Dowding, P. J.; Rogers, S. E.; Heenan, R.; Dyer, R. Are Hydrotropes Distinct from Surfactants? *Langmuir* **2011**, *27*, 12346−12353.

(27) Coffman, R. E.; Kildsig, D. O. Hydrotropic Solubilization Mechanistic Studies. *Pharm. Res.* **1996**, *13*, 1460.

(28) Coffman, R. E.; Kildsig, D. O. Effect of Nicotinamide and Urea on the Solubility of Riboflavin in Various Solvents. *J. Pharm. Sci.* **1996**, *85*, 951−954.

(29) Yang, B.; Hoober-Burkhardt, L.; Krishnamoorthy, S.; Murali, A.; Surya Prakash, G. K.; Narayanan, S. R. High-Performance Aqueous Organic Flow Battery with Quinone-Based Redox Couples at Both Electrodes. *J. Electrochem. Soc.* **2016**, *163*, A1442−A1449.

(30) Pan, F.; Wang, Q. Redox Species of Redox Flow Batteries: A Review. *Molecules* **2015**, *20*, 20499−20517.

(31) Subramanian, D.; Anisimov, M. A. Phase Behavior and Mesoscale Solubilization in Aqueous Solutions of Hydrotropes. *Fluid Phase Equilib.* **2014**, *362*, 170−176.

(32) Permatasari, A.; Lee, W.; Kwon, Y. Performance Improvement by Novel Activation Process Effect of Aqueous Organic Redox Flow Battery Using Tiron and Anthraquinone-2,7-Disulfonic Acid Redox Couple. *Chem. Eng. J.* **2020**, *383*, No. 123085.

(33) Booth, J. J.; Omar, M.; Abbott, S.; Shimizu, S. Hydrotrope Accumulation around the Drug: The Driving Force for Solubilization and Minimum Hydrotrope Concentration for Nicotinamide and Urea. *Phys. Chem. Chem. Phys.* **2015**, *17*, 8028−8037.

(34) Kim, J. Y.; Kim, S.; Papp, M.; Park, K.; Pinal, R. Hydrotropic Solubilization of Poorly Water-Soluble Drugs. *J. Pharm. Sci.* **2010**, *99*, 3953−3965.

(35) Da Silva, R. C.; Spitzer, M.; Da Silva, L. H. M.; Loh, W. Investigations on the Mechanism of Aqueous Solubility Increase Caused by Some Hydrotropes. *Thermochim. Acta* **1999**, *328*, 161−167.
(36) Balasubramanian, D.; Srinivas, V.; Gaikar, V. G.; Sharma, M. M. Aggregation Behavior of Hydrotropic Compounds in Aqueous Solution. *J. Phys. Chem. A.* **1989**, *93*, 3865−3870.
(37) Bauduin, P.; Renoncourt, A.; Kopf, A.; Touraud, D.; Kunz, W. Unified Concept of Solubilization in Water by Hydrotropes and Cosolvents. *Langmuir* **2005**, *21*, 6769−6775.
(38) Duarte, F.; Geng, T.; Marloie, G.; Al Hussain, A. O.; Williams, N. H.; Kamerlin, S. C. L. The Alkaline Hydrolysis of Sulfonate Esters: Challenges in Interpreting Experimental and Theoretical Data. *J. Org. Chem.* **2014**, *79*, 2816−2828.
(39) O'Neil, M. J. *The Merck Index*, 15th ed.; The Royal Society of Chemistry: Cambridge, 2013.
(40) Evans, D. H. One-Electron and Two-Electron Transfers in Electrochemistry and Homogeneous Solution Reactions. *Chem. Rev.* **2008**, *108*, 2113−2144.
(41) Bard, A. J.; Faulkner, L. R. Fundamentals and Applications. *Electrochem. Methods* **2001**, *2*, 580−632.
(42) Carlson, E. D.; Majda, M. Electrochemistry of TEMPO: An Assessment of the Water Diffusion Constant in the Aqueous Liquid/Vapor Interfacial Region. *J. Solid State Electrochem.* **2013**, 3083−3091.
(43) Fan, H.; Zhang, J.; Ravivarma, M.; Li, H.; Hu, B.; Lei, J.; Feng, Y.; Xiong, S.; He, C.; Gong, J.; Gao, T.; Song, J. Radical Charge Population and Energy: Critical Role in Redox Potential and Cycling Life of Piperidine Nitroxyl Radical Cathodes in Aqueous Zinc Hybrid Flow Batteries. *ACS Appl. Mater. Interfaces* **2020**, *12*, 43568−43575.
(44) Treimer, S.; Tanga, A.; Johnson, D. C. A Consideration of the Application of Koutecky-Levich Plots in the Diagnoses of Charge-Transfer Mechanisms at Rotated Disk Electrodes. *Electroanalysis* **2002**, *14*, 165−171.
(45) Samiey, B.; Cheng, C. H.; Wu, J. Effects of Surfactants on the Rate of Chemical Reactions. *J. Chem.* **2014**, *2014*, 1−14.
(46) Rajanna, K. C.; Reddy, K. N.; Kumar, U. U.; Sai Prakash, P. K. A Kinetic Study of Electron Transfer from L-Ascorbic Acid to Sodium Perborate and Potassium Peroxy Disulphate in Aqueous Acid and Micellar Media. *Int. J. Chem. Kinet.* **1996**, *28*, 153−164.
(47) Subba Rao, P. V.; Krishna Rao, G.; Ramakrishna, K.; Rambabu, G.; Satyanarayana, A. Kinetics of Some Electron-Transfer Reactions of Iron(III)-2,2′-Bipyridyl Complex. Micellar Effect of Sodium Dodecyl Sulphate. *Int. J. Chem. Kinet.* **1997**, *29*, 171−179.
(48) Rodríguez, A.; Del Mar Graciani, M.; Balahura, R.; Moyá, M. L. Micellar Effects on the Electron Transfer Reaction within the Ion Pair [(NH3)5Co(N-Cyanopiperidine)]3+/[Fe(CN) 6]4-. *J. Phys. Chem. B.* **1996**, *100*, 16978−16983.
(49) Rubio-Garcia, J.; Kucernak, A.; Parra-Puerto, A.; Liu, R.; Chakrabarti, B. Hydrogen/Functionalized Benzoquinone for a High-Performance Regenerative Fuel Cell as a Potential Large-Scale Energy Storage Platform. *J. Mater. Chem. A* **2020**, *8*, 3933−3941.
(50) VanGelder, L. E.; Petel, B. E.; Nachtigall, O.; Martinez, G.; Brennessel, W. W.; Matson, E. M. Organic Functionalization of Polyoxovanadate−Alkoxide Clusters: Improving the Solubility of Multimetallic Charge Carriers for Nonaqueous Redox Flow Batteries. *ChemSusChem* **2018**, *11*, 4139−4149.
(51) Swinehart, D. F. The Beer-Lambert Law. *J. Chem. Educ.* **1962**, *39*, 333−335.
(52) Scrucca, L. GA: A Package for Genetic Algorithms in R. *J. Stat. Software* **2013**, *53*, 1−37.
(53) Scrucca, L. On Some Extensions to GA Package: Hybrid Optimisation, Parallelisation and Islands Evolution. *R J.* **2017**, *9*, 187−206.
(54) Efron, B. Bootstrap Methods: Another Look at the Jackknife. *Ann. Stat.* **1979**, *7*, 1−26.

https://doi.org/10.1021/acsomega.1c05133
ACS Omega 2021, 6, 30800−30810